Asymmetric Impact of Tropical SST Anomalies on Atmospheric Internal Variability over the North Pacific

WILBUR Y. CHEN AND HUUG M. VAN DEN DOOL

Climate Prediction Center, NOAA/NWS/NCEP, Washington, D.C.

(Manuscript received 5 December 1995, in final form 16 August 1996)

ABSTRACT

A substantial asymmetric impact of tropical Pacific SST anomalies on the internal variability of the extratropical atmosphere is found. A variety of diagnoses is performed to help reveal the dynamical processes leading to the large impact. Thirty-five years of geopotential heights and 29 years of wind fields analyzed operationally at the National Centers for Environmental Prediction (NCEP), formerly the National Meteorological Center, and three sets of 10-yr-long perpetual January integrations run with a low-resolution NCEP global spectral model are investigated in detail for the impact of the SST anomalies on the blocking flows over the North Pacific. The impact on large-scale deep trough flows is also examined.

Both the blocking and deep trough flows develop twice as much over the North Pacific during La Niña as during El Niño winters. Consequently, the internal dynamics associated low-frequency variability (LFV), with timescales between 7 and 61 days examined in this study, display distinct characteristics: much larger magnitude for the La Niña than the El Niño winters over the eastern North Pacific, where the LFV is highest in general.

The diagnosis of the localized Eliassen–Palm fluxes and their divergence reveals that the high-frequency transient eddies (1–7 days) at *high* latitudes are effective in forming and maintaining the large-scale blocking flows, while the *mid*latitude transients are less effective. The mean deformation field over the North Pacific is much more diffluent for the La Niña than the El Niño winters, resulting in more blocking flows being developed and maintained during La Niña by the high-frequency transients over the central North Pacific.

In addition to the above dynamical process operating on the high-frequency end of the spectrum, the local barotropic energy conversion between the LFV components and the time-mean flows is also operating and playing a crucial role. The kinetic energy conversion represented by the scalar product between the E vector of the low-frequency components and the deformation D vector of the time-mean flow reveals that, on average, the low-frequency components extract energy from the time-mean flow during La Niña winters while they lose energy to the time-mean flow during El Niño winters. This local barotropic energy conversion on the low-frequency end of the spectrum, together with the forcing of the high-frequency transients on blocking flows on the high-frequency end, explain why there is a large difference in the magnitude of low-frequency variability between the La Niña and the El Niño winters.

1. Introduction

a. Basic questions and definitions

The atmospheric internal variability discussed in this paper refers to those temporal and spatial variations developing while the flow system is subjected to constant external forcing conditions. For a perpetual GCM run, the variability generated on all timescales is easily understood to be caused by internal dynamics, since the forcing conditions are held constant. For the real atmosphere, variability is not all internal. In addition to the repetitive annual cycle, the slowly varying anomalous forcings external to the atmospheric system inevitably generate additional variability. The total variability therefore consists of two parts, internal and external. Taking a seasonal mean of a meteorological variable for example, its interannual variability consists of a climate signal (externally forced) and climate noise [variability that occurs even when the change in forcing is negligible, e.g., Lau (1981)]. For high-frequency synoptic-scale transients, one can also envision that the external forcing conditions affect their magnitude, the location of their principal tracks, etc.

Isolating climate signal from climate noise is an important task in climate prediction. It has been known to be a formidable, if not impossible, challenge (e.g., Leith 1973; Madden 1976; Trenberth 1985; Chervin 1986). The goal of this article is not to find out how much external–internal variability there is in a seasonal mean. We attempt to tackle a simpler question: When the external conditions change from El Niño to La Niña forcing, is there a corresponding and substantial change in the characteristics of variability on timescales smaller than a season? Using blocking flows to exemplify the

Corresponding author address: Dr. Wilbur Y. Chen, Prediction Branch, Climate Prediction Center, NOAA/NWS/NMC, Washington, DC 20233.
E-mail: wd51wc@sun1.wwb.noaa.gov

question, would blocking flows develop more or less frequently during El Niño or La Niña winters?

To answer the above question, the internal variability of the real atmospheric flow is defined here as the departure from a slowly varying time-mean flow, not the traditional anomalies that are defined as the departures from the longtime climatological mean. With this definition, the above question is then reduced to, Is there a substantial impact of tropical Pacific SST anomalies on the extratropical atmospheric internal variability?

The response of the time-mean flow to external forcing has been well documented and qualitatively understood in various frameworks (e.g., Opsteegh and Van den Dool 1980; Hoskins and Karoly 1981; Horel and Wallace 1981; Blackmon et al. 1983; Cubash 1985; Miyakoda et al. 1986). However, to what extent a tropical forcing modifies the shorter timescale internal variability of the extratropical atmosphere is less clear. For instance, as we asked earlier, is there a significant change in the frequency of blocking-flow development over the North Pacific when the external forcing is changed, say, from El Niño– to La Niña–type tropical SST forcing? Furthermore, is there also a significant impact on the large-scale deep trough flow developments? If there is a large difference, why?

In a recent article, Chen and Van den Dool (1995c) show that, for widely different basic flows, the low-frequency variability exhibits distinct characteristics: much smaller magnitude for a North Pacific cyclonic basic flow than for an anticyclonic basic flow. These results based on 8 yr of recent National Centers for Environmental Prediction (NCEP) data were obtained without explicit reference to tropical SST. In the present paper, using a variety of diagnostic tools and 35 yr of geopotential heights and 29 yr of wind fields, we aim to establish that, due to the large impact of tropical SST anomalous forcing, the atmospheric internal variability over the North Pacific, exemplified by the large-scale blocking and deep trough flows, is subjected to drastic change in magnitude and other characteristics. The role that ENSO's warm/cold events play in severe weather development over the Pacific/North American sector can therefore be expected to be very pronounced.

Atmospheric internal variability in midlatitudes has a wide range of temporal and spatial scales. Besides synoptic-scale weather phenomena, blocking flows are perhaps the most striking examples. A blocking flow disrupts the normal passage of weather systems and diverts a normally westerly jet stream into a strong meridional current, resulting in outbreaks of arctic air and devastating deep freeze in wintertime. Due to its prominence and possible outcome of economic loss and human suffering, we will focus our attention on large-scale blockings, as well as the ''opposite'' deep trough flows, and to what extent their magnitude and frequency is modified by El Niño and La Niña.

b. Brief overview of the literature

Although blocking flows have been the subject of much research, the current prediction skill of blocking by comprehensive numerical models is still far from satisfactory. For instance, early dynamical extended-range forecast experiments (Tracton et al. 1989; Chen and Van den Dool 1995a) indicate that a large portion of the unskillful forecasts can be traced back to the model's inability to predict the evolution of blocking events beyond a few days into the forecast.

Several dynamical processes have been identified regarding the formation and maintenance of blocking flows. Recent diagnostic and observational studies (e.g., Green 1977; Holopainen et al. 1982; Shutts 1983; Egger and Schilling 1983; Hoskins et al. 1983; Metz 1986; Trenberth 1986; Mullen 1987; Hoskins and Sardeshmukh 1987; Lau 1988; Nakamura and Wallace 1990) indicate that the synoptic-scale transient eddies play a crucial role. Another theory is that the normal mode instability of the three-dimensional basic flow (Frederiksen 1982, 1983) can set up and grow into a dipole block. Blocks have also been interpreted as localized spherical modons (e.g., Tribbia 1984; Verkley 1984; Haines and Marshall 1987) or nearly stationary solutions to the equations of atmospheric motion (e.g., Branstator and Opsteegh 1989; Anderson 1993).

The impact of tropical SST forcing on the extratropical blocking flows is less documented and understood. Ferranti et al. (1994) studied the impact of a variety of localized SST anomalies on blocking. Namias (1986) and von Storch (1987) indicated that, during El Niño–type forcing, the extratropical low-frequency variability (LFV) is smaller than during La Niña forcing, implicitly implying less development of blocking flows during El Niño winters. Due to the importance of the blocking flows in affecting a regional short-term climate, it is imperative to make a detailed study as to how the tropical SST anomalous forcing impacts the development of the extratropical blocking flows. In addition to blocking flows, their counterpart, the large-scale deep trough flows, can also affect severely the short-term climate. And, if there is a large impact of El Niño/La Niña on deep troughs, what are the leading operating dynamical processes?

During El Niño winters, the synoptic-scale transients are known to be organized in part by the North Pacific time-mean negative height anomaly such that the storm tracks shift slightly equatorward and extend substantially eastward, along with the similarly strengthened, much eastward extended subtropical jet. During La Niña winters, the synoptic-scale transients are diverted instead around the northern flank of the North Pacific time-mean positive anomaly. The question is, Do the high-frequency transients in El Niño/La Niña conditions have the same effectiveness in forcing blocked flow? According to Trenberth (1986) and Branstator (1992), the high-frequency transients are usually not configured

optimally for forcing the LFV unless some ''organizing mechanism'' makes them effective. Therefore, it is important to find out in what situation the transients result in more blocking flows.

Furthermore, the degree of diffluence in the mean deformation field should be substantially different between El Niño and La Niña winters, due to the fact that their time-mean flow response over the North Pacific to the tropical SST forcing is distinct. It is expected then that the growth of blocking flows should also exhibit large differences (Farrell 1989). Therefore, besides the nonlinear feedback of synoptic-scale transients onto the blocking flows, the barotropic energy conversion between low-frequency components and their time-mean flows could play a role in the magnitude of the low-frequency variability (Mak 1991; Branstator 1992; Cai and Van den Dool 1994).

c. Outline of the present study

Using 35 yr of geopotential heights, 29 yr of wind fields, and three sets of GCM experiments simulating El–Niño type, La Niña–type, and climatological forcing, respectively, this article attempts to document the El Niño–Southern Oscillation (ENSO) cycle's large impact on both blocking and deep trough flows over the North Pacific. In addition to presenting evidence that the internal variability of the extratropical atmosphere is drastically modified by the polarity of the tropical SST forcing, the dynamical processes leading to this large change will also be explored. After a brief description of the data used and the method of analysis in section 2, the time-mean response of the extratropical atmosphere to the tropical SST forcing will be presented in section 3, and the results of SST impacts on the atmospheric internal variability will be shown in sections 4 and 5 for blocking and deep trough flows, respectively. Strong support from GCM experiments, revealing new insight that the internal variability is indeed behaving very differently under El Niño and La Niña external forcing, will be shown in section 6. The relationship between high-frequency transients and blocking flows will be described in section 7, and further discussed in the light of Shutts's (1983) eddy straining mechanism (involving the localized Eliassen–Palm flux) in section 8. The barotropic kinetic energy conversion between LFV components and time-mean flows, represented by the scalar product of E and D vectors (Mak and Cai 1989), will be assessed in section 9, followed by a summary and concluding remarks in section 10.

2. Data and methodology

The primary data used are the NCEP operationally analyzed geopotential heights at 500 mb (Z500) from 1957 to 1993 and wind fields at 250 mb (U250 and V250) from 1965 to 1993. The Climate Analysis Center maintains a daily Z500 dataset, from 1957 to the present, compiled from a National Center for Atmospheric Research (NCAR) CD-ROM and recent NCEP analyses. The historic twice-daily Z500 fields were averaged to form a daily dataset. A few missing height fields in the 1950s were filled in with linear interpolation. Wind fields are missing more often, and some months had to be rejected altogether. For further detail the reader is referred to Chen and Van den Dool (1995b) and the references therein.

As described below a substantial impact of tropical Pacific SST anomalous forcing on blocking flows was found in this historic dataset. In order to substantiate the finding, a low-resolution NCEP medium-range forecast model (T40L18) (Sela 1980; Kanamitsu 1989; Kalnay et al. 1990) was run to generate three GCM simulations. These are long ''perpetual'' January experiments: one with above normal tropical SST (SSTA run), one with below normal tropical SST (SSTB run), and one with roughly climatological tropical SST (SSTC run), which was represented by the average of the SST in the SSTA and SSTB runs. The initial conditions were the same (16 January 1992) and all boundary conditions, except SSTs, are the same for all three experiments and remained fixed for 3600 days of model integration. The SSTA fields were taken from December 1991 and January 1992 (an El Niño winter); that is, the mean of these 2 months was taken as SSTA. Similarly, SSTB was constructed from the mean of December 1988 and January 1989 (a La Niña winter). The difference between SSTA and SSTB is more than 4°C over the equatorial Pacific east of the dateline. Details will be shown later in section 6.

To diagnose why there is such a large impact of ENSO on the atmospheric internal variability, winds at 250 mb (U250 and V250) were used for the evaluations of localized Eliassen–Palm fluxes and their divergence following Trenberth (1986). The kinetic energy conversion between LFV components and the time-mean flows were also calculated from these wind fields.

The atmospheric low-frequency fluctuations we are concerned with in this study are mainly the disturbances with timescales shorter than 61 days and longer than 7 days. Here we would like to emphasize again our unconventional treatment of disturbances. What we are interested in are low-frequency disturbances embedded in 61-day time-mean flow (which is known to be ''polarized'' by the tropical SST anomalous forcing). In our treatment, the presumed externally forced time-mean flow element is thus filtered out from consideration. The disturbances under consideration are not the conventional flow anomalies from climatology, but departures from a 61-day running mean.

To isolate internal disturbances, we form first the daily anomaly by removing the 30-yr climatology (1961 to 1990) from the daily data at each grid point. Then a 61-day high-pass running mean filter was applied on these daily anomalies for each winter (1 November–31 March). A 7-day low-pass running mean filter is next

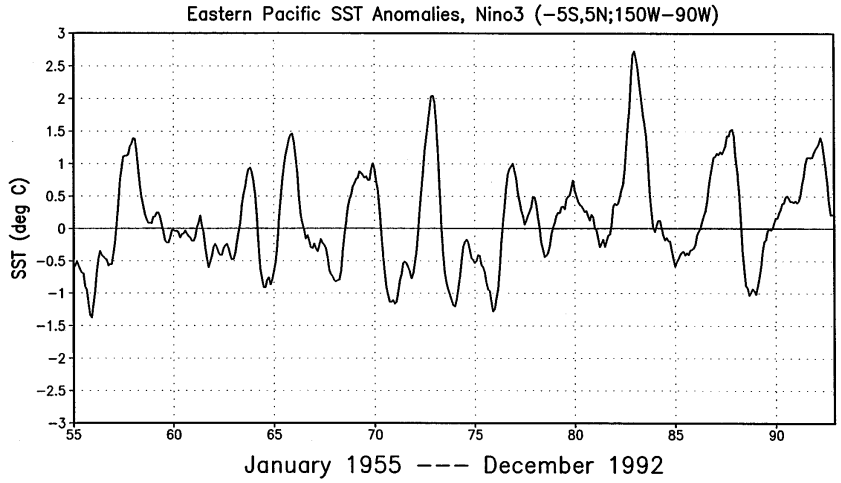

FIG. 1. Sea surface temperature time series over Niño-3. A low-pass temporal filter of 5 months has been applied to the monthly mean data.

applied to these 61-day high-pass filtered data. With these simple operations, the fluctuations with timescales longer than 61 days and shorter than 7 days are crudely filtered out of the time series. The final data used for each winter are from 1 December to 28 February.

The synoptic-scale disturbances are also considered in sections 7 and 8 where the relationship between high-frequency transients and blocking flows are explored through localized Eliassen–Palm flux vector diagnoses. For that purpose, a 7-day high-pass running mean filter is applied to the daily anomalies to form the 1–7-day timescale range time series. The wind field data are similarly treated with n-day running mean high-pass or low-pass filter, with n = either 61 or 7.

3. Time-mean response to El Niño and La Niña SST forcing

The NCEP's SST ''reanalysis'' for the period 1950–92 (Smith et al. 1996) was used to construct SST anomalies for the eastern tropical Pacific area. Niño-3, which covers the domain of 5°S to 5°N and 150°W to 90°W, was chosen to indicate the phase of the ENSO interannual variation. Niño-3 SST anomalies from 1955 to 1992 are shown in Fig. 1. Based on this SST anomaly time series, El Niño and La Niña boreal winters can be identified. Eight cases for each type of forcing were chosen. Labeling the year by January, the El Niño December–February (DJF) winters chosen are 1958, 1966, 1970, 1973, 1977, 1983, 1987, and 1992. The La Niña DJFs are 1962, 1965, 1968, 1971, 1974, 1976, 1985, and 1989.

The time-mean circulation associated with El Niño– and La Niña–type forcing can therefore be obtained in a straightforward manner. Significant differences in the time-mean flow over the North Pacific can be seen in Fig. 2, which shows the Z500 composites for the La Niña and El Niño DJFs. Sharper difference in the time-mean response of the Northern Hemisphere to the El Niño and La Niña forcing can be seen from the anomaly composites shown in Fig. 3, in which the 30-yr climatology (1961–90) has been subtracted. In Fig. 3, a Pacific–North America (PNA)-like pattern is seen. We can also observe 1) a much larger magnitude of the time-mean anomaly over the North Pacific for the El Niño DJFs than the La Niña DJFs, −70 m versus +50 m; 2) the teleconnection to other anomaly centers is also stronger during El Niño DJFs. All of these features will be supported by the GCM experiments in section 6.

The above results are in very good agreement with those reported by Horel and Wallace (1981). With the time-mean response to the SST forcing well documented, we next try to document the impact of the tropical Pacific SST anomalous forcing on blocking flows, and in addition on deep trough flows over the North Pacific sector.

4. ENSO impact on blocking flows

Blocking flow has been defined in various ways (e.g., Rex 1950; Dole 1986; Tibaldi and Molteni 1990; Anderson 1993). For our purpose, a simple threshold definition of blocking is found to be satisfactory. The definition of a blocking high, in this article, is based on a criterion involving the deviation from a running 61-day time mean, not the conventional height anomaly such as that defined by Dole (1986). With the subtraction of the 61-day time-mean anomaly, the inherent advantage (for blocked flows) of a positive departure on top of an already positive 61-day time-mean anomaly (such as during La Niña) is eliminated.

At a given grid point on a given day, a blocking high is identified if the 7–61-day band-pass filtered Z500 disturbance is greater than 200 m. A search for blocked flows anywhere between 40° and 60°N was conducted.

Two examples of a blocking high thus defined are

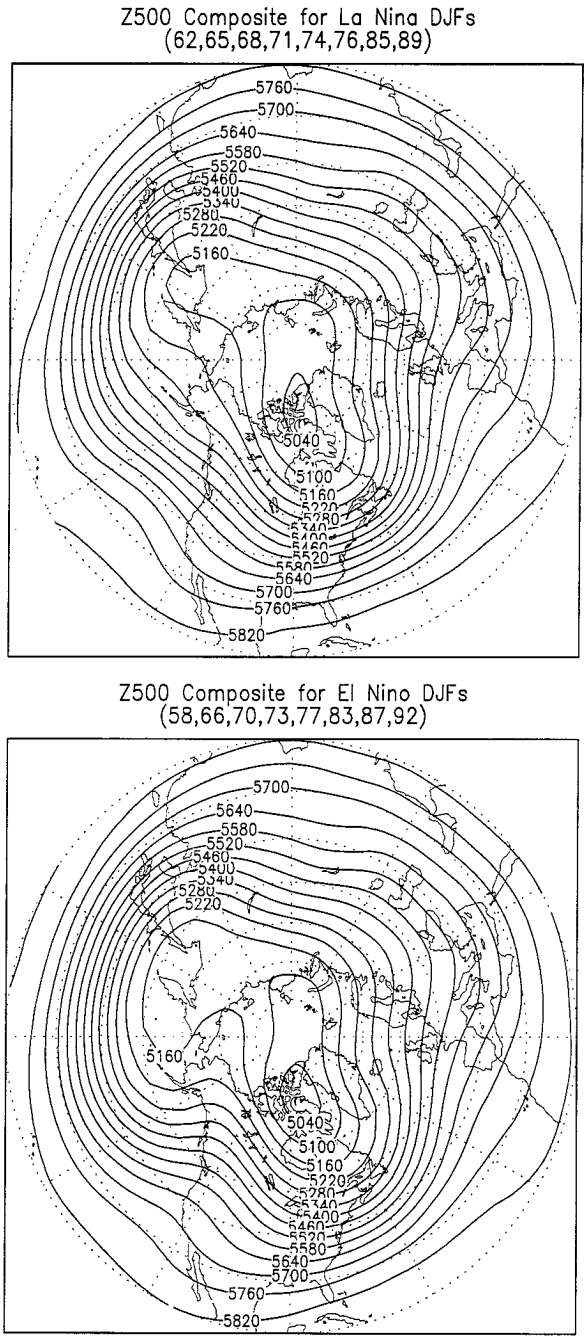

FIG. 2. The Z500 composite. Upper panel: La Niña DJFs. Lower panel: El Niño DJFs. Contour unit is in meters.

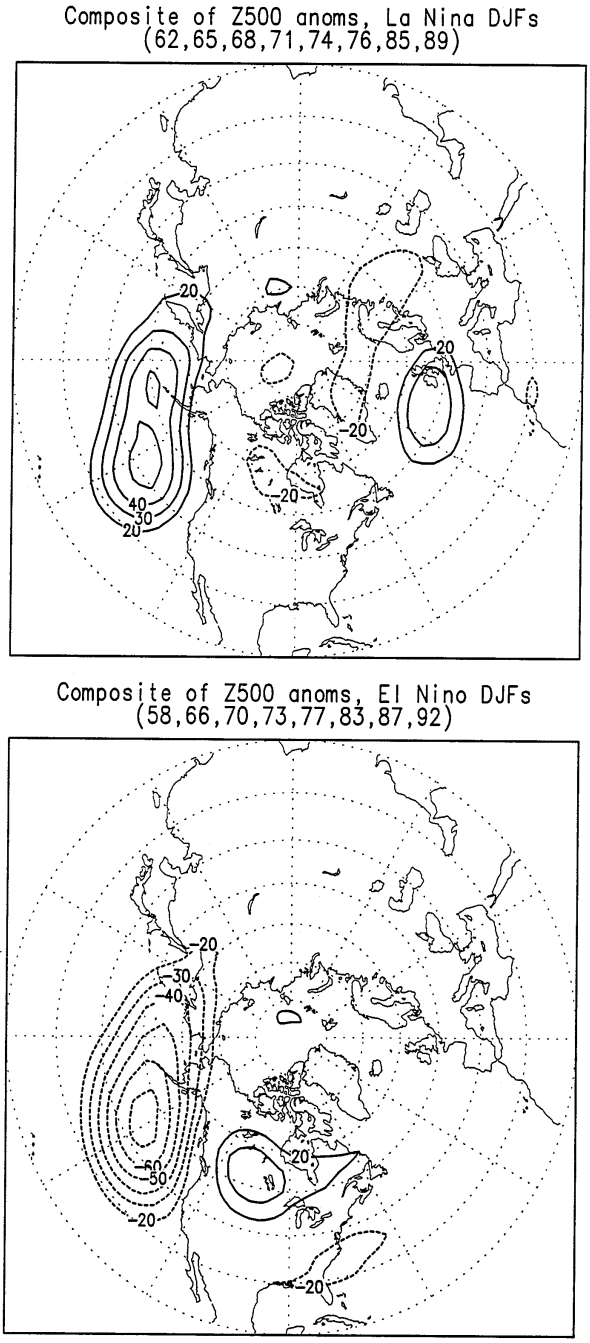

FIG. 3. Comparison of the Z500 anomaly composite. The climatology of 1961–90 is employed, with solid curve for positive anomaly and dashed for negative. Contour unit is in meters.

shown in Fig. 4, where over the North Pacific a dipole-blocking flow is shown in the upper panel and a blocking ridge shown in the lower panel. As the term implies, the dipole-blocking flow has a clear center of negative height south of the large positive height. The positive center of the dipole-blocking is usually located at high latitudes. The blocking ridge (lower panel, Fig. 4) is more rare and has one positive center, usually in mid-latitudes. For brevity, we will refer to both varieties as blocks.

Figure 5 presents the percentage of time that blocking flow is present. The solid curve shows the result when all 35 DJF winters were considered, the solid circles for the 8 La Niña winters, and the open circles for the 8 El Niño DJFs. Very convincingly, the blocking flows develop substantially less than average during El Niño

winters, while substantially more than average during La Niña winters. West of the date line, blocking frequency is at least twice as high for La Niña as for El Niño winters. Between 180° and 140°W, where the occurrence of blocking flow is at a maximum in general, the blocking frequency for the La Niña winters is also much more than for the El Niño winters; 15% versus 10% of the time.

5. ENSO impact on deep trough flows

The same 7–61-day bandpass filtered Z500 fields were searched for large negative disturbances. The percentage of time that a negative disturbance exceeds −200 m was similarly binned as a function of longitude. Figure 6 presents the results. The solid curve represents again the 35-winter average, solid circles the La Niña, and open circles the El Niño result. The stratification of deep troughing frequency is even more remarkable than the blocking frequency. Clearly, deep troughs are much more common during La Niña DJFs, while quite rare during El Niño DJFs. Between 160° and 140°W, where the maximum of deep trough development is located, the difference in frequency of occurrence is 15% versus 7%, more than twice as much for La Niña as for El Niño winters.

Therefore, the tropical Pacific SST anomaly not only affects the seasonal time-mean circulation, as shown in Figs. 2 and 3, but also modifies dramatically the characteristics of the internal low-frequency variability over the North Pacific, such as blocking and deep trough flows.

Before considering why there is such a large difference, we would like to point out another distinction. In Fig. 7 we place the development frequency of blocking and deep trough flows, copies from Figs. 5 and 6, together in one figure for La Niña DJFs (the upper panel) and El Niño DJFs (the lower panel). Consistent with early estimates of skewness by White (1980), it is clear from Fig.7 that blocking flows generally develop much more frequently than deep trough flows over the central North Pacific. Why? What dynamical process lead to this large distinction?

Given these observations, there are three major questions we would like to consider. 1) Why do blocking flows develop much more frequently during La Niña than El Niño winters? 2) Why do deep trough flows also develop much more frequently during La Niña than El Niño winters? 3) Why, in general, do blocking flows develop much more frequently than deep trough flows over the central North Pacific?

Before considering these questions, we would like to substantiate the results obtained so far from observations by some GCM experiments.

6. GCM results

An inescapable shortcoming of the observed data (the NCEP operational analyses) is their limited number of

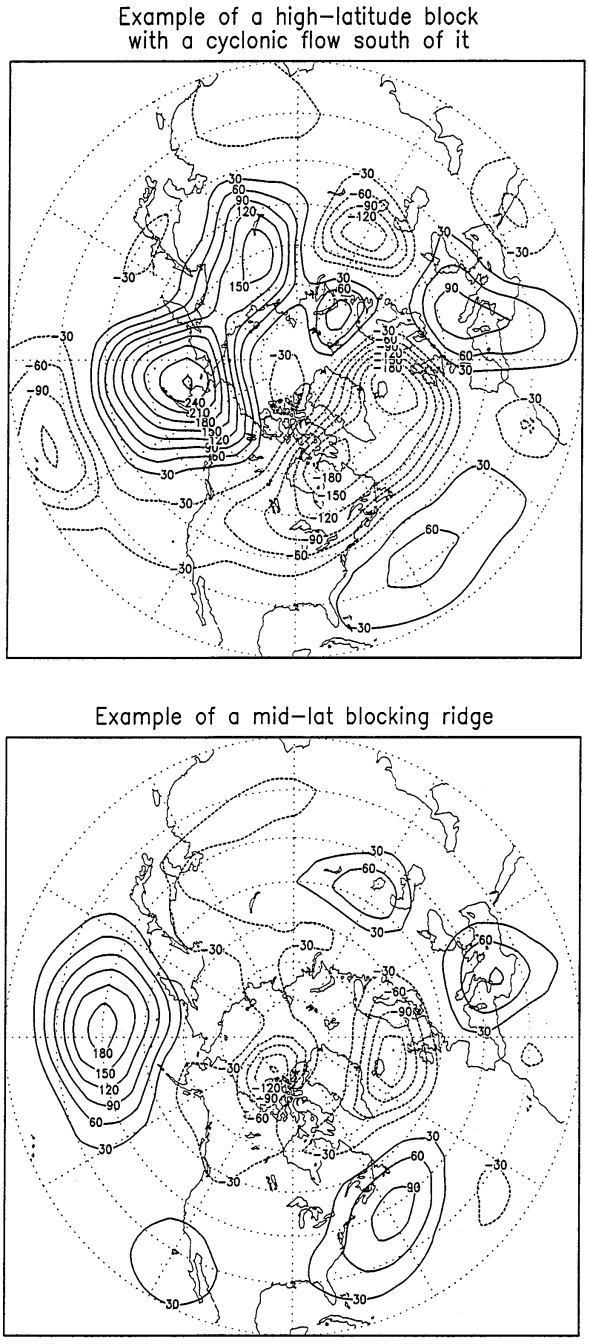

FIG. 4. Two examples of blocking flow over the North Pacific. Time series at each grid point has been bandpass filtered to isolate fluctuations with timescales of 7–61 days; solid curve is for positive deviation from the 61-day running mean and dashed is for negative (m).

El Niño/La Niña events. The results shown so far appear to be robust. Yet a consistent behavior from a large volume of independent data will certainly elevate confidence. Will GCM simulations yield the same picture? In order to find out, we conducted three sets of 3600-day long SST impact experiments. The GCM used and

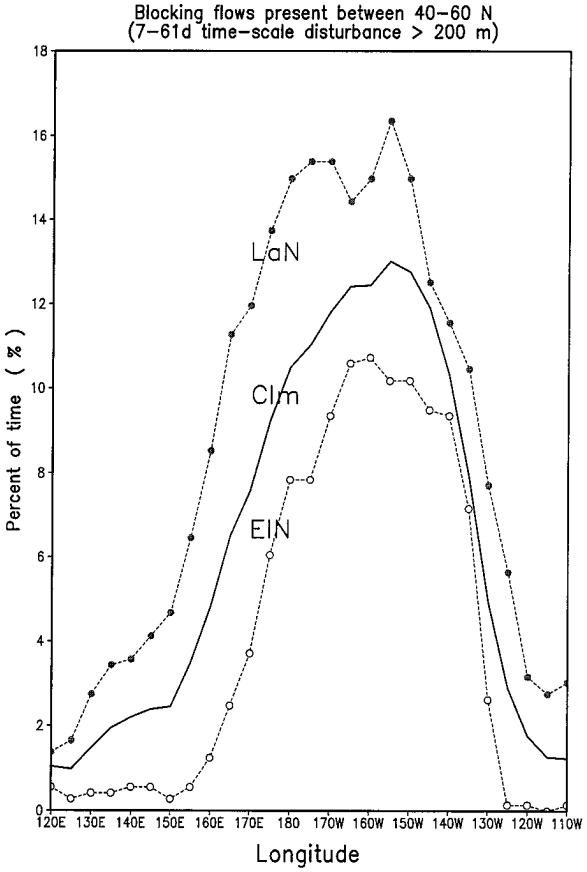

FIG. 5. Comparisons of percentage of time that blocking flows were developed: solid curve for all 35 winters, closed circles for La Niña DJFs, and open circles for El Niño DJFs.

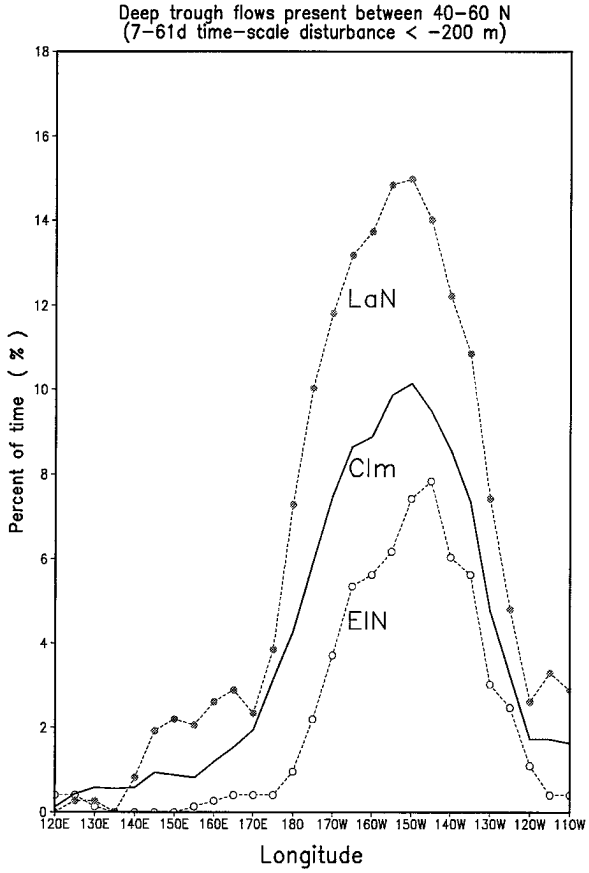

FIG. 6. Same as Fig. 5 except for deep trough flows being present.

the experimental design have been described in section 2. The SSTA run simulates the El Niño general circulation, while the SSTB run simulates the La Niña flows. The sea surface temperature difference between SSTA and SSTB is shown in Fig. 8, where a significant 4°C difference can be seen over the equatorial Pacific east of the date line. Very little difference exceeding 1°C can be spotted in other parts of the globe.

The first 50 days of integration were discarded due to the drift of the model climate. Figure 9 shows the difference of the mean Z500 between SSTB and SSTC runs (upper panel) and between SSTA and SSTC runs (lower panel). The SSTB (SSTA) displays a prominent positive (negative) height anomaly in the North Pacific, and similar to observed (Fig. 3), the positive for La Niña is weaker than the negative for El Niño. The teleconnection to the U.S. southeast center is stronger for El Niño than for La Niña, agreeing again with an aspect of the observed pattern in Fig. 3. The resemblance between GCM runs (Fig. 9) and the observed (Fig. 3) gives us confidence that the SSTA and SSTB runs simulate the El Niño and La Niña time-mean flow conditions fairly well in the sense that they generate an impact on the mean flow in the right direction and of the right magnitude.

The impact of SSTs on model development of blocking and deep trough flows was obtained in the same way as used above for the observed cases and is summarized in Fig. 10. Note that the height threshold used for the GCM data had to be reduced from 200 m to 150 m. This is because the model's variability on various timescales is only about 75% of the real atmosphere's variability (Chen and Van den Dool 1995b). In Fig. 10, the open circles represent the percentage of time that blocking flows are present between 40° and 60°N, and solid circles represent similar results for the deep trough flows; the upper panel is for the SSTB run and the lower panel for the SSTA run. In agreement with observations, a much higher frequency of both blocking and deep trough flows is found for the SSTB than for the SSTA run. And, in general, blocking flow develops much more frequently than deep trough flow over the central North Pacific.

Compared to Fig. 7 (observed), the GCM blocking and deep trough flows develop more narrowly over the Gulf of Alaska area instead of spreading over most of the North Pacific as observed. This model systematic error is consistent with the difference in behavior of

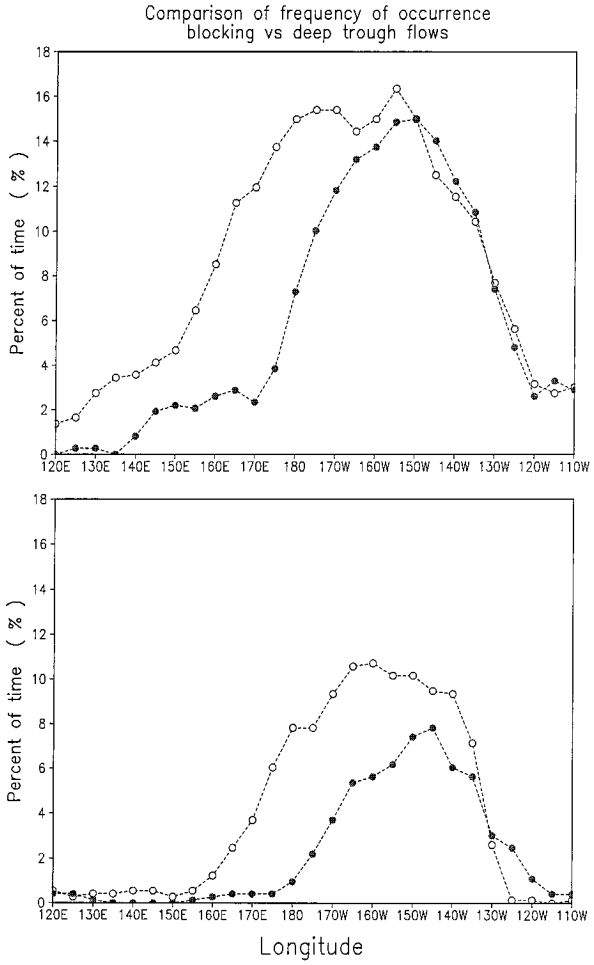

FIG. 7. Contrast of development frequency between blocking flows (open circles) and deep trough flows (solid circles); upper panel is for La Niña DJFs, and lower panel is for El Niño DJFs.

low-frequency anomalies in the NCEP Medium-Range Forecast model and reality as reported recently by Chen and Van den Dool (1995b).

7. High- and low-frequency variability contrasts

The blocking and deep trough flows presented above for the GCM-generated data are unambiguously associated with the internal variability, because the boundary forcing conditions are held constant throughout the integrations. Those representing ''observed,'' presented in sections 4 and 5, can also be reasonably treated as internal variability, because they are within either the El Niño or the La Niña group, with each group subjected to a similar type of SST forcing. It is even easier for the synoptic-scale disturbances to rationalize that they are part of the internal dynamic variability. Yet as we will show in the coming two sections, this high- and lower-frequency variability can be organized and modified indirectly by the tropical SST anomalous forcing.

Before presenting formal diagnostics, we would like

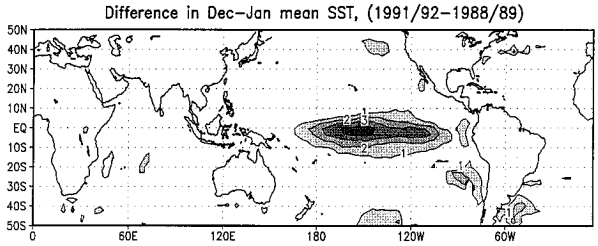

FIG. 8. Difference in December–January mean SST between 1991–92 and 1988–89 (°C).

to contrast the relationship between the high- and lower-frequency transients for the La Niña and the El Niño winters. Synoptic-scale transients with timescales of 1–7 days will be referred to here as the high-frequency components and those with 7–61 day timescales as low-frequency components. The high-frequency variance (HFV) and low-frequency variance (LFV) were obtained separately for the La Niña and El Niño DJFs and are contrasted side by side in Fig. 11.

An immediate impression from this figure is the overwhelming magnitude of the LFV for the La Niña DJFs compared to that of the El Niño DJFs; namely, 200 dm^2 versus 140 dm^2. The corresponding GCM results, as shown in Fig. 12, offer strong support to this large difference. The above large difference in LFV is consistent with the earlier results showing that the frequency of both blocking and deep trough flows is much higher for La Niña than for El Niño DJFs. Figures 11 and 12 also show that the LFV is located at the end of the principal storm track. In addition, large HFV over the Aleutians is associated with large LFV (for La Niña DJFs), while smaller HFV appears in conjunction with smaller LFV (for El Niño DJFs) over the eastern North Pacific. Whether or not this is consistent with the understanding that the synoptic transients decay sometimes into lower-frequency fluctuations remains to be seen. In the following sections we will more formally investigate the HFV–LFV interaction.

8. Shutts's eddy straining mechanism

Mechanisms explaining the development and maintenance of blocking flows have been the subject of much research. Feedback of the synoptic-scale transients to the blocking flow has gained prominence as a leading maintenance mechanism. We here pursue the idea of Shutts (1983), who explains blocking from a preexisting diffluent flow and high-frequency eddies approaching from upstream. Following Hoskins et al. (1983), but using Trenberth's formulation (1986), we calculated the barotropic zonal component of the local Eliassen–Palm flux vector, denoted here by **E,** as follows:

$$\mathbf{E} = \left[\frac{1}{2}(\overline{v'^2} - \overline{u'^2}),\ -\overline{u'v'}\right],$$

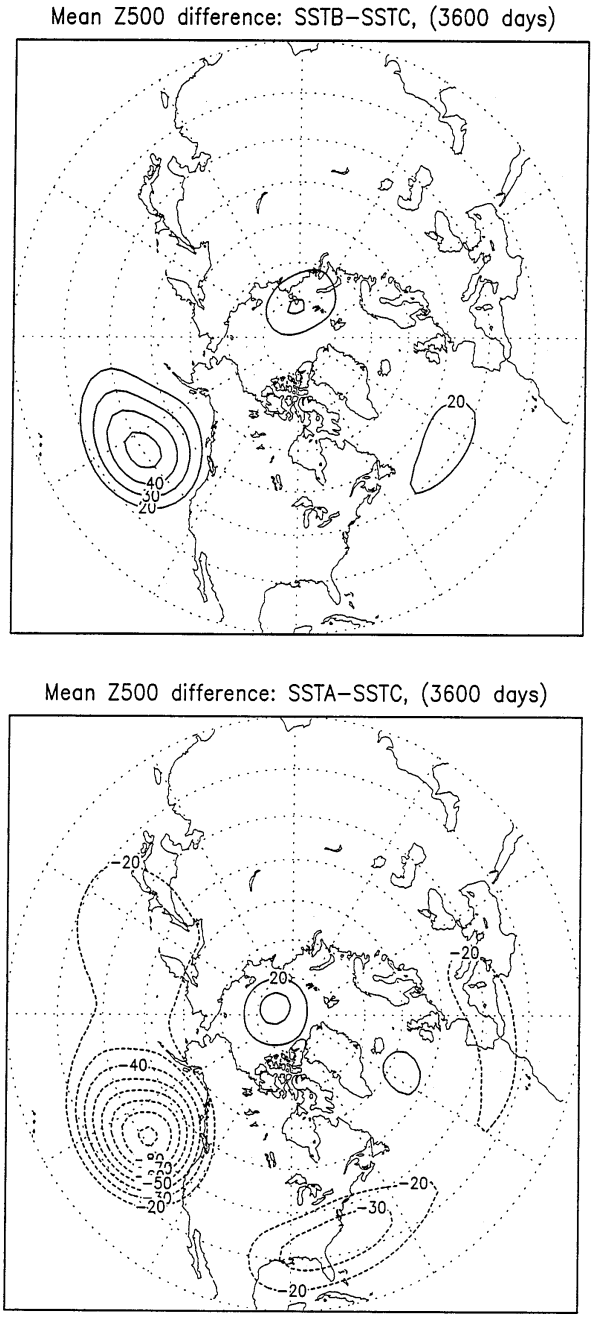

FIG. 9. Similar to Fig. 3 except for the GCM experiments. SSTC denotes perpetual run with climatological SST conditions; SSTA denotes above and SSTB below climatological SST conditions.

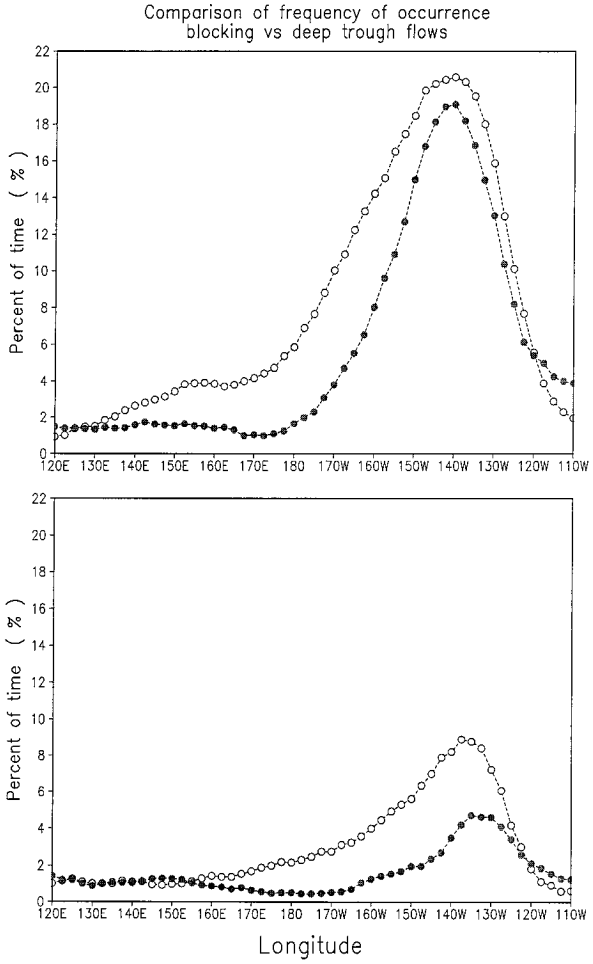

FIG. 10. Similar to Fig. 7 except for the perpetual GCM runs.

where u' and v' are the 1–7-day high-frequency wind components and the overbar denotes temporal averaging. The result based on all 29 yr of wind data is shown in the upper panel of Fig. 13, in which we also present the divergence of **E** in the lower panel.

The dominant feature in the lower panel of Fig. 13 is the acceleration of the climatological jet stream along 45°N by the forcing of the high-frequency transients, with a maximum divergence of **E** between 170° and 180°W. Another important feature in the lower panel is the convergence of **E** at higher latitudes north of about 55°N, implying deceleration of the mean westerly flows by the actions of the high-frequency transients. The deceleration also turns slightly northeastward east of the date line.

The orientation of **E** (the upper panel) in this deceleration zone is perhaps most noteworthy. Focusing our attention over the area of 55°–65°N and 160°E–130°W, we can see a clockwise rotation of the **E** vector from the 9 o'clock to the 3 o'clock position, implying a gradual change from $|u'|>|v'|$ to $|u'|<|v'|$, or in other words, a compressing of $|u'|$ and a stretching of $|v'|$ over this deceleration area. Shutts's eddy straining mechanism (1983) appears to be operating in this area: the eddies are being deformed systematically by the large-scale ambient flow in such a way that they feed back to decelerate the westerlies and help to form and maintain blocking flows (Shutts 1983; Trenberth 1986). The vector **E** and its convergence together suggest that the high-frequency transient eddies at high latitudes are much

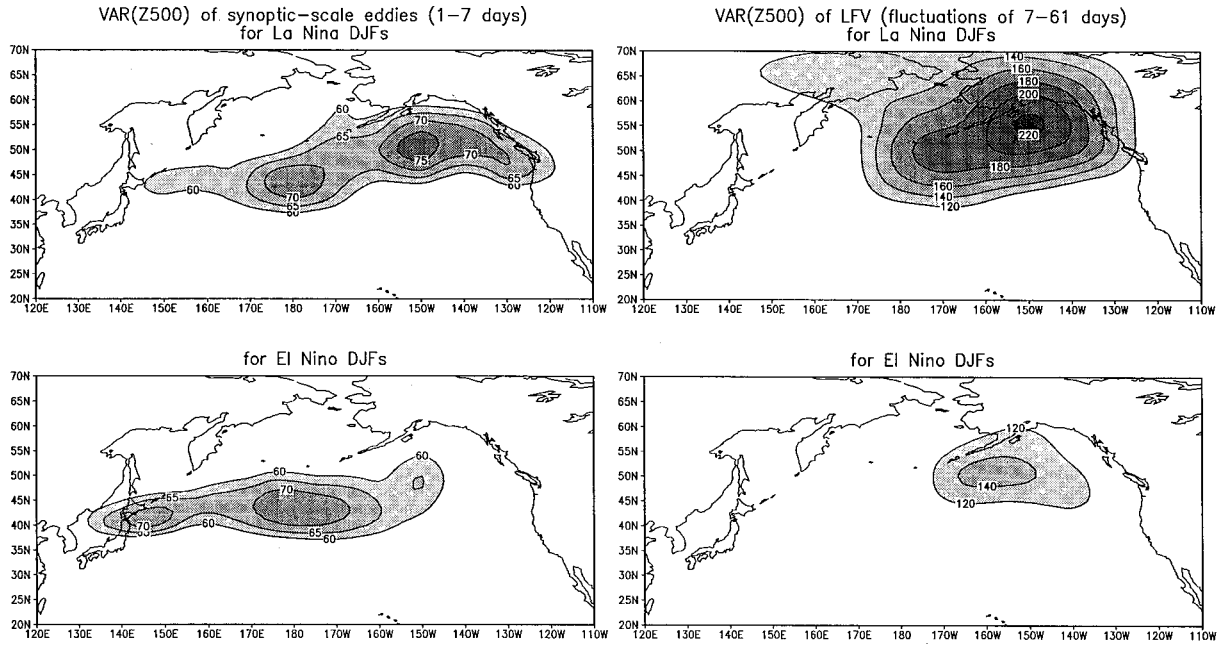

FIG. 11. Comparisons of Z500 variance for all 35 winters between high- and low-frequency disturbances, and between La Niña and El Niño winters (dm^2).

more effective in forcing and maintaining the blocking flows than at midlatitudes. Indeed, Fig. 14 upholds this interpretation. The figure presents the percentage of time during all DJFs that a blocking flow develops at 60°N, contrasted with that developed at 45°N. Near the date line blocks occur about three times as often at 60°N than at 45°N. High-latitude blocks occur more than four times as often as midlatitude blocks near 150°W, where the deceleration of the zonal wind is largest, as shown in Fig. 13.

From these results, we are in a better position to see why during El Niño winters the blocking flows are greatly reduced and why during La Niña winters the blocking flows are greatly increased. Responding to enhanced

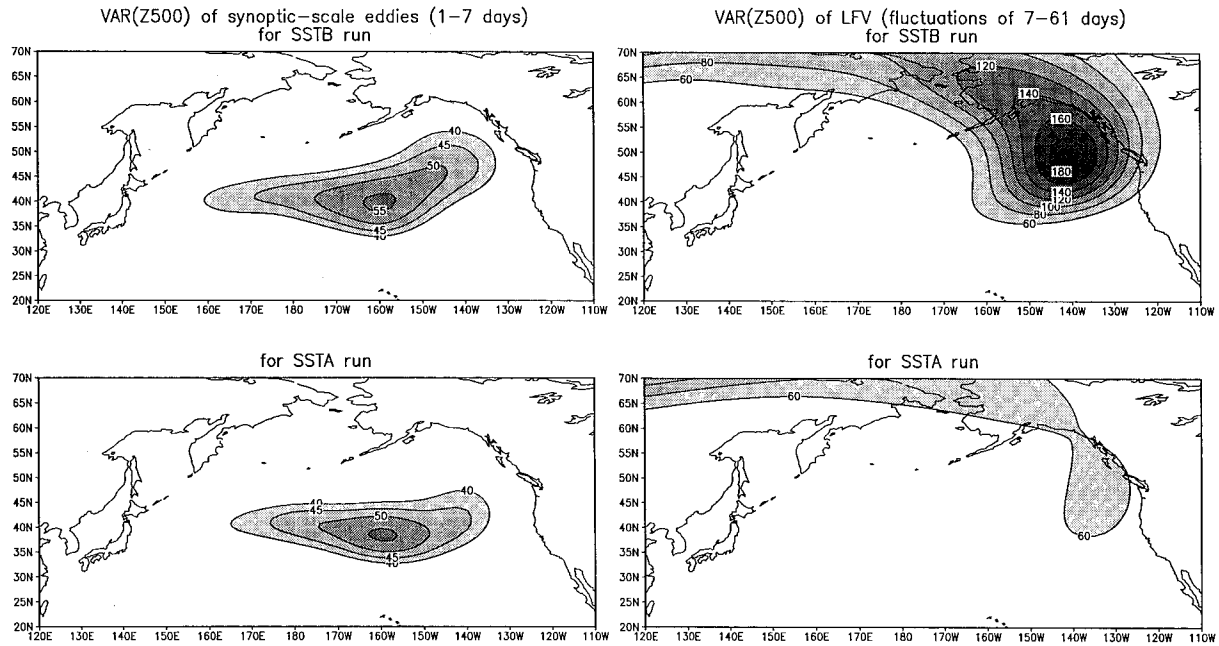

FIG. 12. Similar to Fig. 11 except for the GCM runs.

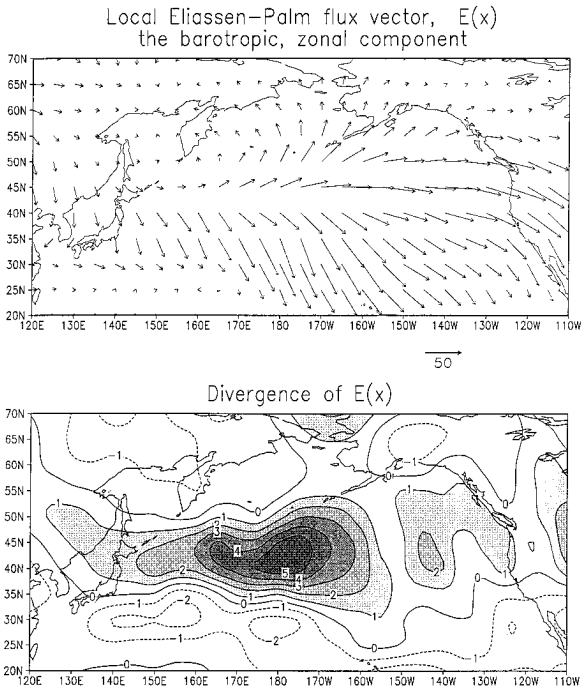

FIG. 13. The barotropic, zonal component of the local Eliassen–Palm flux vector $\mathbf{E}(x)$ (upper panel, in units of $m^2\ s^{-2}$) and the divergence of $\mathbf{E}(x)$ (lower panel, in units of $m\ s^{-1}\ day^{-1}$). Results obtained from all 29 winters.

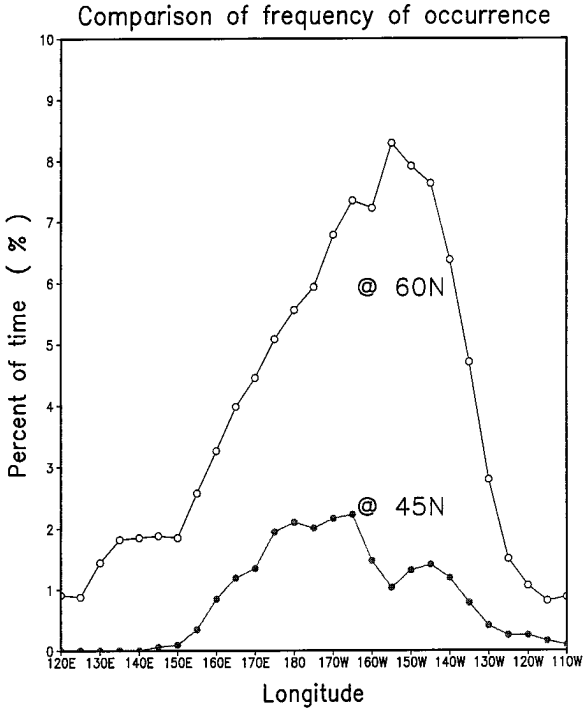

FIG. 14. The percentage of time that blocking flows developed at high latitudes (open circles) compared to those at midlatitudes (closed circles). Results obtained from all 35 winters.

convection over the tropical Pacific during El Niño winters, the subtropical jet strengthens and extends much eastward, as shown in the bottom panel of Fig. 15. Accompanying this strengthening of the jet is a cyclonic time-mean anomalous flow over the North Pacific. The storms are then diverted along tracks more equatorward as well as more eastward than normal. At these latitudes and with less diffluent flow over the North Pacific, as shown in Fig. 16 (bottom right), the high-frequency transient eddies are not effective in forming and maintaining blocking flows, explaining why blocking flows are observed less than normal, as shown in Fig. 5.

On the other hand, during La Niña winters, an anomalous anticyclonic time-mean flow, accompanied by a weaker and shorter subtropical jet, diverts storm tracks northeastward. At higher latitudes and with the help of much more diffluent flows over the North Pacific as shown in Fig. 16 (top right), the high-frequency transient eddies would presumably become very effective in forming and maintaining the blocking flows, thus explaining the much higher than normal frequency of blocking, as shown in Fig. 5.

Other pieces of evidence regarding the effectiveness of high-latitude, high-frequency transients in forcing blocked flow are presented in Figs. 17 and 18. In Fig. 17, while much larger divergence of the Eliassen–Palm (E–P) flux vector (acceleration) is observed over the eastern North Pacific for the El Niño DJFs (bottom), as expected, the high-latitude convergence for the La Niña

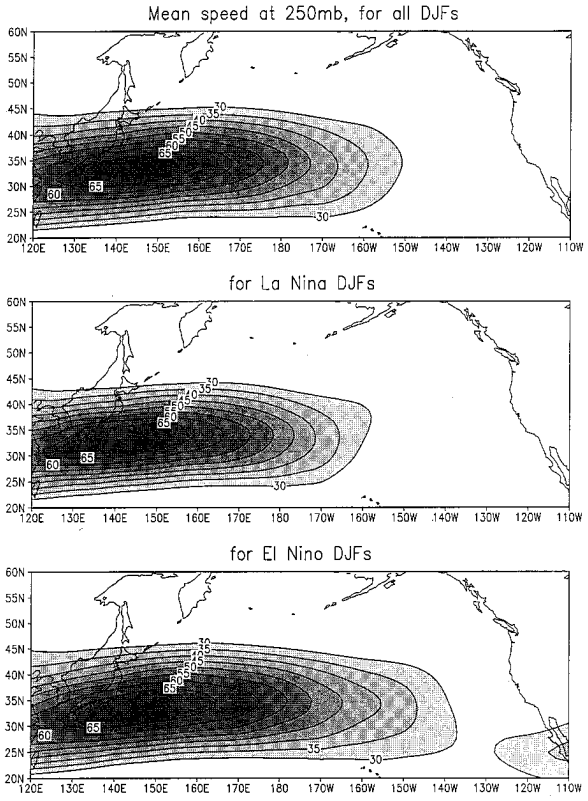

FIG. 15. Comparisons of subtropical jet strength ($m\ s^{-1}$).

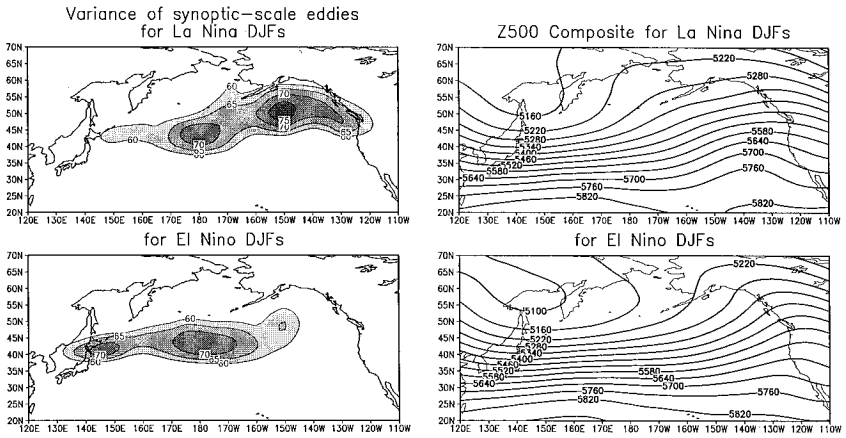

FIG. 16. Comparison of mean diffluence (the rhs panels), as implied by the Z500 full field, between La Niña and El Niño winters. The respective principal storm tracks are duplicated on the 1hs panels from Fig. 11.

DJFs (top) is observed to be larger, implying more deceleration of the westerly flows during La Niña DJFs. Figure 18 compares the blocking frequency at 60°N and 45°N separately for the La Niña (the upper panel) and the El Niño DJFs (the lower panel). That the low-frequency transients are much more common at high latitudes for both groups is apparent. Taking La Niña DJFs, for example, at 150°W, almost 10 times more blocking flows developed at 60°N than at 45°N. For the El Niño DJFs, the difference in blocking frequency is not as dramatic as for the La Niña case, yet a clear difference between 60°N and 45°N is observed.

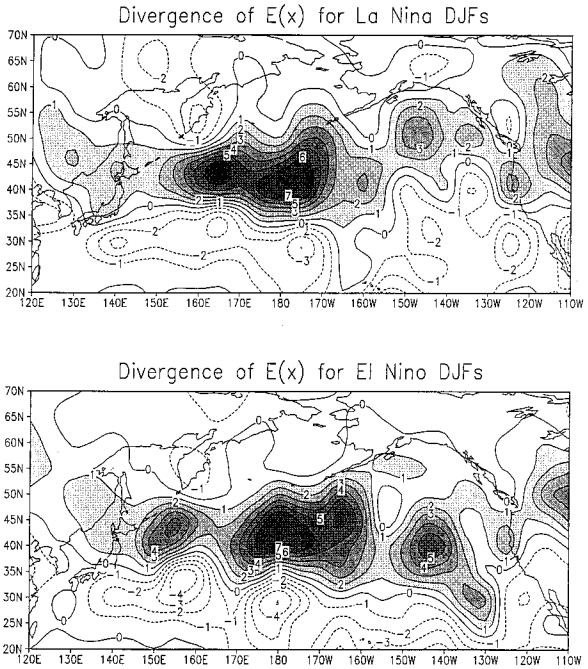

FIG. 17. Similar to the lower panel of Fig. 13 except for 6 La Niña DJFs (top) and 6 El Niño DJFs (bottom).

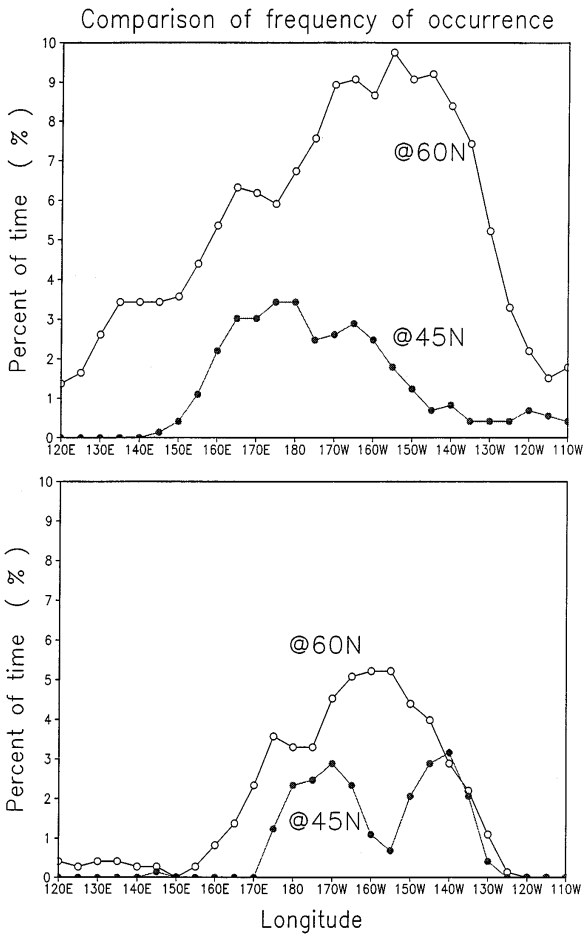

FIG. 18. Similar to those of Fig. 14 except for La Niña DJFs (upper panel) and El Niño DJFs (lower panel).

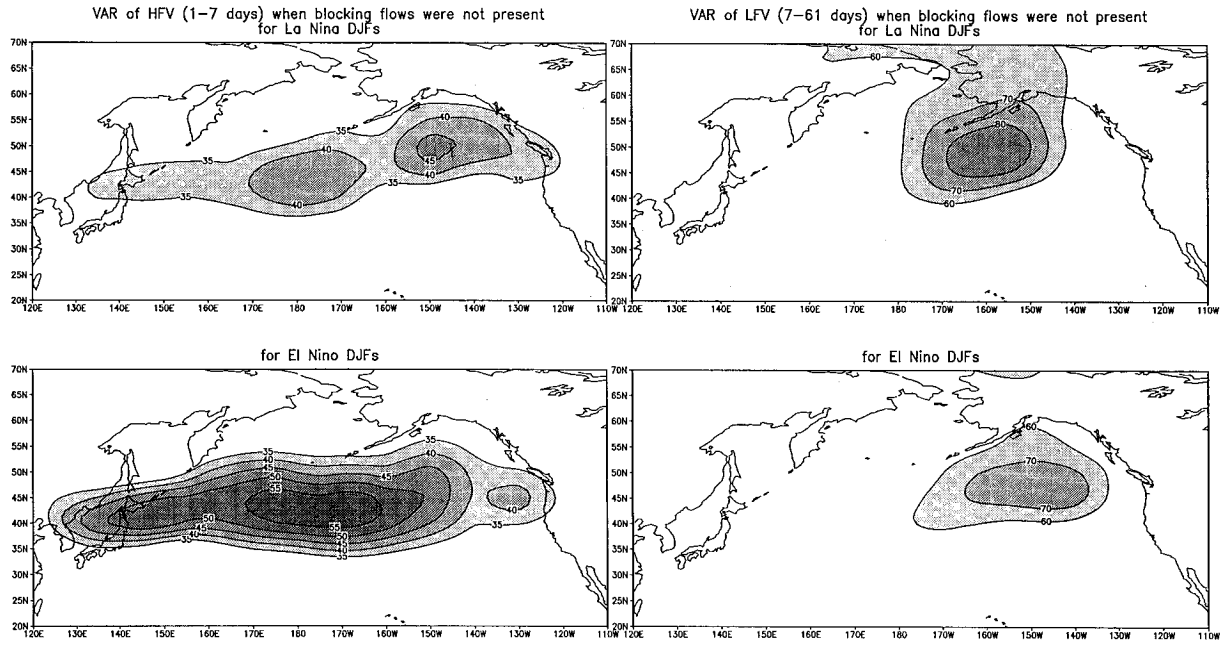

FIG. 19. Comparisons of variances when blocking flows were not present over the North Pacific (dm^2).

So far we have studied why there is much more blocking flow development during La Niña than El Niño winters and why the presence of the high-frequency transients is a possible dynamical process leading to many more high-latitude blocking flows in general. But we have not yet considered why there are also many more deep trough flows over the eastern North Pacific during La Niña winters than El Niño winters. The following diagnosis is intended to explore this issue.

9. Role of the local barotropic energy conversion

Another view of the relationship between high- and low-frequency transients is shown in Fig. 19, where we present the HFV (1–7 days) and LFV (7–61) when blocking flows were *not* present over the North Pacific, so that the LFV is due *mainly* to deep trough flows. The purpose is to see what is left of the relationship when blocking flows associated high- and low-frequency fluctuations are excluded from the picture.

The upper panels are for the La Niña DJFs and the lower panels for El Niño DJFs. Note that while the La Niña's HFV is much smaller than that of the El Niño's (left-hand side panels), its corresponding LFV is much larger (right-hand side panels). Therefore, the significant difference in LFV cannot be due alone to the forcing of the high-frequency transients. An additional dynamical process must be operating to account for the difference in LFV over the eastern North Pacific.

Simmons et al. (1983) suggest that much of the LFV of the Northern Hemisphere wintertime general circulation is associated with disturbances that derive their energy from the zonally varying basic state through barotropic instability. This idea has been highlighted further by Palmer (1988) and Molteni and Palmer (1993). It is thus plausible that the local barotropic energy conversion between the zonally varying time-mean flows and the low-frequency components of both polarities might help to account for the large differences in the LFV shown in Figs. 11 and 19.

The dynamical process of local barotropic energy conversion is investigated here by examining the kinetic energy equation. Using here the exact notations and definitions of Mak and Cai (1989), the growth rate of the local perturbation energy is governed by the scalar product, $\mathbf{E}\cdot\mathbf{D}$, in the following equation:

$$\epsilon_t = -\mathbf{V}\cdot\nabla\epsilon + \mathbf{E}\cdot\mathbf{D} - 2r\epsilon - \mathbf{v}\cdot\nabla p, \qquad (1)$$

where

$$\epsilon = \frac{1}{2}(u^2 + v^2), \qquad \mathbf{v} = (u, v), \qquad \mathbf{V} = (U, V),$$

where lower (upper) case refers to perturbation (mean flow) and

$$E = \left[\frac{1}{2}(v^2 - u^2), -uv\right], \qquad (2)$$

$$D = (U_x - V_y, V_x + U_y). \qquad (3)$$

Finally, p is pressure and r is a linear dissipation constant.

As discussed by Mak and Cai (1989), the mean-flow advection of the perturbation energy and the ageostrophic pressure work do not contribute to the change of the global energetics. The dissipation term always decreases the perturbation energy, thus leaving only $\mathbf{E}\cdot\mathbf{D}$

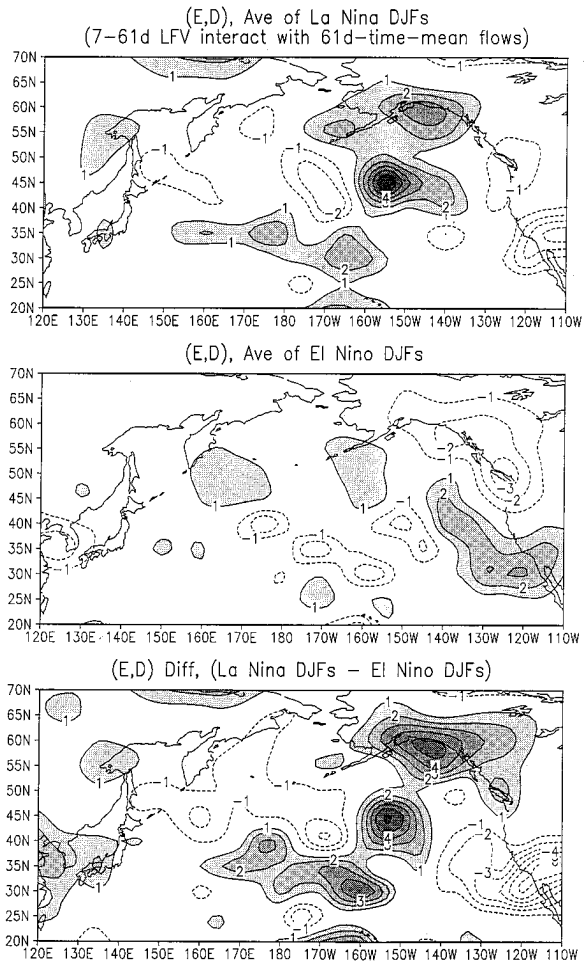

FIG. 20. Comparisons of the inner products of the **E** and **D** vectors [(d m s^{-1})^2 s^{-1}].

for possible maintenance. The **E** vector quantifies the local structure and the strength of the transient eddies, while the **D** vector defines the deformation field of the time-mean flow in which the eddies are embedded.

To evaluate the barotropic energy conversion between the time-mean flows and the LFV components, we treated as perturbations the disturbances (of both polarities now) with timescales between 7 and 61 days and the 61-day low-pass filtered wind fields as the time-mean flow. The **E**-vector was calculated through (2) and the **D**-vector through (3) by using finite difference. As was done earlier for the local E–P flux diagnosis, wind fields at 250-mb level were used.

Due to a shorter record and missing historical wind data, we have only 6 El Niño events (1966, 1973, 1977, 1983, 1987, 1992), and 6 La Niña events (1968, 1971, 1974, 1976, 1985, 1989). We have already shown that, for time-mean flow as different as La Niña winters from El Niño winters, the associated variability exhibits distinct characteristics. We would like to find out whether or not the barotropic energy conversion between the low-frequency components and the time-mean flows also helps to account for this large difference.

The average inner product **E**·**D** was calculated and is shown separately in Fig. 20 for the La Niña DJFs (the upper panel) and the El Niño DJFs (the middle panel). The difference between them is shown in the bottom panel. Remarkable differences in **E**·**D** can be seen over the eastern North Pacific. For the La Niña deformation conditions (upper panel), the LFV transients tend to extract energy from the time-mean flows, resulting in larger magnitude of LFV. For the El Niño deformation conditions, the energy conversion points to more decaying of the LFV transients into the time-mean flow (middle panel). Large differences in **E**·**D** between La Niña and El Niño DJFs, as shown in the bottom panel, clearly suggest that, over the eastern North Pacific, the extraction of the perturbation LFV energy from the time-mean flow is much greater during La Niña than El Niño winters.

Figure 20 leaves open the possibility of whether the change of sign of the energy conversion is due to a change in mean flow, or due to a change in structure of the low-frequency eddies. We thus redid our calculation with **E** from all winters, and **D,** as before, from the La Niña or El Niño winters. This yields Fig. 21, which is like a smooth version of Fig. 20. It thus seems that the change in mean flow is the agent leading to a sign reversal in barotropic energy conversion.

Therefore, while the feedback mechanism alone (the high-frequency transient eddies acting to form and maintain blocking flows) can account for some of the large difference in LFV magnitude over the eastern North Pacific, the barotropic energy conversion between the time-mean flows and the low-frequency transients also helps in accounting for the large differences in LFV, as shown in Figs. 11 and 19.

10. Summary and conclusions

While the impact of tropical Pacific SST anomalies on the time-mean response of the northern winter extratropical atmosphere is well documented and understood, their impact on subseasonal variability is less clear. Does blocking flow develop with distinct frequency for different forcing conditions? Specifically, would blocking flows develop more frequently during La Niña than El Niño winters? Here, the blocking flow is defined as a positive disturbance on top of the slowly varying time-mean flow, which is known to be impacted by the external boundary conditions. The blocking flow considered here is distinct from the time-mean flow, thus void of the elements directly associated with the external forcing conditions, and therefore is considered to be a part of the internal dynamic variability. The blocking flow analyzed here is different from the conventional large positive anomalies, such as investigated by Dole (1986).

Based on Niño-3 SST anomalies, 8 El Niño and La Niña winters were identified. Data from 1957 to 1993 went into the study of the impact of ENSO on the sub-

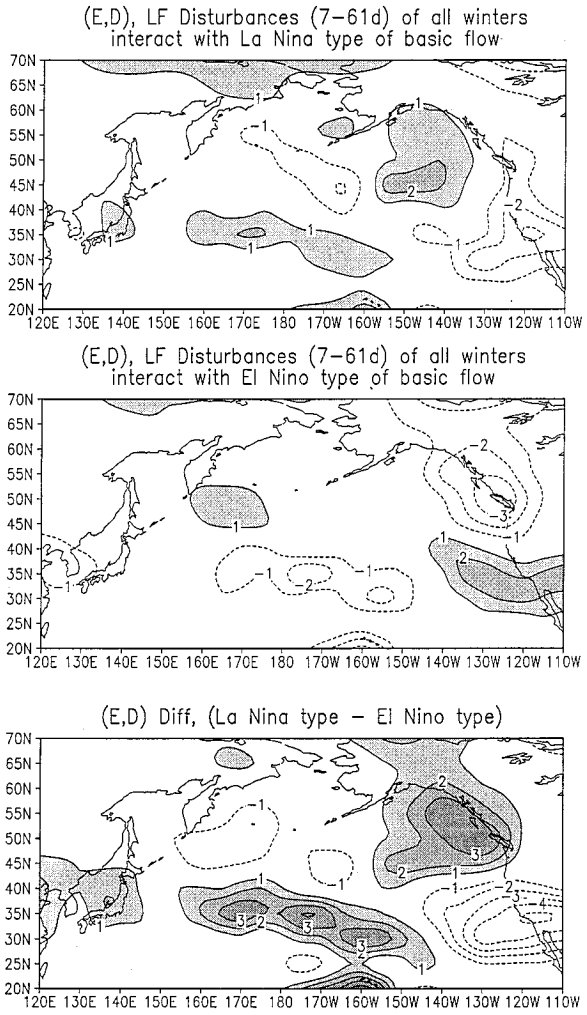

FIG. 21. As in Fig. 20 but now the **E** vector is calculated from low-frequency eddies for all winters.

seasonal variability of 500-mb height as analyzed by NCEP. Because of missing wind fields and shorter available data, only 6 ENSO warm and cold events went into the diagnoses that require the use of U250 and V250.

To support the results found in the real atmosphere, three sets of GCM experiments, simulating the El Niño, La Niña, and climatological general circulations, respectively, were also conducted and analyzed. Another reason for seeking GCM support is that it is fundamentally difficult to split observed variability into internally and externally forced portions. We have attempted to do that by timescale separation. However, in a GCM the boundary condition can be held constant, and all variation is internal.

Using these datasets, a large asymmetric impact of the tropical Pacific SST anomalies on the atmospheric internal variability over the North Pacific was indeed found: a much higher frequency of blocking development and deep trough formation is found during La Niña winters than El Niño winters. A good degree of similarity is found between the observed and the GCM results. Two major dynamical processes leading to this large difference were investigated.

Calculation of the localized Eliassen–Palm fluxes, interpreted in terms of Shutts's (1983) eddy straining mechanism, reveal that, in general, the dominant climatological effect of high-frequency transients is the acceleration of the zonal wind along 45°N and deceleration of zonal flows north of 55°–60°N by the high-frequency transient eddies (HFTEs). At *high* latitudes, where the flow is more diffluent, the HFTEs undergo east–west compression and north–south stretching. Shutts's eddy straining mechanism (1983) appears to operate in that high-latitude area. The HFTEs are being deformed systematically by the large-scale ambient flows in such a way that they feed back to decelerate the westerlies and help to form and maintain the blocking flows in that area (Shutts 1983; Trenberth 1986).

This dynamical process contributes to the large difference in blocking flow development between the El Niño and La Niña phase of the ENSO cycle. For La Niña winters, the synoptic-scale storm activity tends to be organized by the prevailing North Pacific time-mean ridge to go around the northern flank of the ridge. For El Niño DJFs, storm activity tends to be organized to shift slightly southward and extend much more eastward. At the same time, the time-mean deformation field over the North Pacific is much more diffluent for La Niña than El Niño winters. These two factors work together to result in many more blocking flows being developed and maintained by the high-frequency transients over the North Pacific for the La Niña than the El Niño winters.

The diagnosis of local barotropic energy conversion between time-mean flows and low-frequency components of both polarities was also performed through calculation of the inner product of the **E** vector of the low-frequency components and the **D** vector of the time-mean flows. This diagnosis reveals that, on average, the LFV components extract energy from the time-mean flows over the eastern North Pacific during La Niña winters, while they actually lose their energy to the time-mean flow during El Niño winters. This additional dynamical process contributes significantly to the fact that low-frequency variability on the 7–61-day timescales is so much larger in magnitude over the eastern North Pacific for the La Niña winters than the El Niño winters.

We finally note that the $\mathbf{E}\cdot\mathbf{D}$ calculation does not change much when the **E** vector is derived from LFV for all winters (and **D** is for La Niña and El Niño respectively). It thus seems that the change in mean flow is more important for the energy conversion than the redistribution of the eddies themselves.

Acknowledgments. The authors would like to thank Drs. Zoltan Toth and Glen White, and the three anonymous reviewers for their careful reviews of this manuscript and their valuable comments leading to improvements of this

article. The addition of Fig. 21, which makes the analysis more precise, was suggested by one of the reviewers.

REFERENCES

Anderson, J. L., 1993: The climatology of blocking in a numerical forecast model. *J. Climate,* **6,** 1041–1056.

Blackmon, M. L., J. E. Geisler, and E. J. Pitcher, 1983: A general circulation model study of January climate anomaly patterns associated with interannual variation of equatorial Pacific sea surface temperatures. *J. Atmos. Sci.,* **40,** 1410–1425.

Branstator, G., 1992: The maintenance of low-frequency atmospheric anomalies. *J. Atmos. Sci.,* **49,** 1924–1945.

——, and J. D. Opsteegh, 1989: Free solutions of the barotropic vorticity equation. *J. Atmos. Sci.,* **46,** 1799–1814.

Cai, M., and H. M. Van den Dool, 1994: Dynamical decomposition of low-frequency tendencies. *J. Atmos. Sci.,* **51,** 2086–2100.

Chen, W. Y., and H. M. Van den Dool, 1995a: Forecast skill and low-frequency variability in NMC DERF90 experiments. *Mon. Wea. Rev.,* **123,** 2491–2514.

——, and ——, 1995b: Low-frequency anomalies in the NMC MRF model and reality. *J. Climate,* **8,** 1369–1385.

——, and ——, 1995c: Low frequency variabilities for widely different basic flows. *Tellus,* **47A,** 526–540.

Chervin, R. M., 1986: Interannual variability and seasonal climate predictability. *J. Atmos. Sci.,* **43,** 233–251.

Cubash, U., 1985: The mean response of the ECMWF global model to the composite El Niño anomaly in the extended range prediction experiments. *Coupled Ocean–Atmosphere Models,* J. Nihoul, Ed., Elsevier Press, 329–344.

Dole, R. M., 1986: Persistent anomalies of the extratropical Northern Hemisphere wintertime circulation: Structure. *Mon. Wea. Rev.,* **114,** 178–207.

Egger, J., and H. D. Schilling, 1983: On the theory of long-term variability of the atmosphere. *J. Atmos. Sci.,* **40,** 1073–1085.

Farrell, B. F., 1989: Transient development in confluent and diffluent flow. *J. Atmos. Sci.,* **46,** 3279–3288.

Ferranti, L., F. Molteni, and T. N. Palmer, 1994: Impact of localized tropical and extratropical SST anomalies in ensembles of seasonal GCM intergrations. *Quart. J. Roy. Meteor. Soc.,* **120,** 1613–1645.

Frederiksen, J. S., 1982: A unified three-dimensional instability theory of the onset of blocking and cyclogenesis. *J. Atmos. Sci.,* **39,** 969–982.

——, 1983: A unified three-dimensional instability theory of the onset of blocking and cyclogenesis. Part II: Teleconnection patterns. *J. Atmos. Sci.,* **40,** 2593–2609.

Green, J. S. A., 1977: The weather during July 1976: Some dynamical considerations of the drought. *Weather,* **32,** 120–125.

Haines, K., and J. Marshall, 1987: Eddy-forced coherent structures as a prototype of atmospheric blocking. *Quart. J. Roy. Meteor. Soc.,* **113,** 681–704.

Holopainen, E. O., L. Rontu, and N.-C. Lau, 1982: The effect of large-scale transient eddies on the time-mean flow in the atmosphere. *J. Atmos. Sci.,* **39,** 1972–1984.

Horel, J. D., and J. M. Wallace, 1981: Planetary-scale atmospheric phenomena associated with the Southern Oscillation. *Mon. Wea. Rev.,* **109,** 813–829.

Hoskins, B. J., and D. J. Karoly, 1981: The steady linear response of a spherical atmosphere to thermal and orographic forcing. *J. Atmos. Sci.,* **38,** 1179–1196.

——, and P. D. Sardeshmukh, 1987: A diagnostic study of the Northern Hemisphere winter of 1985–6. *Quart. J. Roy. Meteor. Soc.,* **113,** 759–778.

——, I. James, and G. H. White, 1983: The shape, propagation, and mean flow interaction of large-scale weather systems. *J. Atmos. Sci.,* **40,** 1595–1612.

Kalnay, E., M. Kanamitsu, and W. E. Baker, 1990: The NMC global forecast system. *Bull. Amer. Meteor. Soc.,* **71,** 1410–1428.

Kanamitsu, M., 1989: Description of the NMC global data assimilation and forecast system. *Wea. Forecasting,* **4,** 335–342.

Lau, N. C., 1981: A diagnostics study of recurrent meteorological anomalies appearing in a 15-year simulation with a GFDL general circulation model. *Mon. Wea. Rev.,* **109,** 2287–2311.

——, 1988: Variability in the observed midlatitude storm tracks in relation to low-frequency changes in the circulation patterns. *J. Atmos. Sci.,* **45,** 2718–2743.

Leith, C. E., 1973: The standard error of time-averaged estimates of climate means. *J. Appl. Meteor.,* **12,** 1066–1069.

Madden, R. A., 1976: Estimates of the natural variability of time-averaged sea-level pressure. *Mon. Wea. Rev.,* **104,** 942–952.

Mak, M., 1991: Dynamics of an atmospheric blocking as deduced from its local energetics. *Quart. J. Roy. Meteor. Soc.,* **117,** 477–493.

——, and M. Cai, 1989: Local barotropic instability. *J. Atmos. Sci.,* **46,** 3289–3311.

Metz, W., 1986: Transient cyclone-scale vorticity forcing of blocking highs. *J. Atmos. Sci.,* **43,** 1467–1483.

Miyakoda, K., J. Sirutis, and J. Ploshay, 1986: One-month forecast experiments—Without anomaly boundary forcings. *Mon. Wea. Rev.,* **114,** 2363–2401.

Molteni, F., and T. N. Palmer, 1993: Predictability and finite-time instability of the northern winter circulation. *Quart. J. Roy. Meteor. Soc.,* **119,** 269–298.

Mullen, S. L., 1987: Transient eddy forcing of blocking flows. *J. Atmos. Sci.,* **44,** 3–22.

Nakamura, H., and J. M. Wallace, 1990: Observed changes in the baroclinic wave activity during the life cycles of low-frequency circulation anomalies. *J. Atmos. Sci.,* **47,** 1100–1117.

Namias, J., 1986: Persistence of flow patterns over North America and adjacent ocean sectors. *Mon. Wea. Rev.,* **114,** 1368–1383.

Opsteegh, J. D., and H. M. Van den Dool, 1980: Seasonal differences in the stationary response of a linearized primitive equation model: Prospects for long-range weather forecasting? *J. Atmos. Sci.,* **37,** 2169–2185.

Palmer, T. N., 1988: Medium and extended range predictability and stability of the Pacific/North American mode. *Quart. J. Roy. Meteor. Soc.,* **114,** 691–713.

Rex, D. F., 1950: Blocking action in the middle troposphere and its effects upon regional climate I. An aerological study of blocking action. *Tellus,* **2,** 196–211.

Sela, J. G., 1980: Spectral modeling at the National Meteorological Center. *Mon. Wea. Rev.,* **108,** 1279–1292.

Shutts, G. J., 1983: The propagation of eddies in diffluent jet streams: Eddy vorticity forcing of blocking flow fields. *Quart. J. Roy. Meteor. Soc.,* **109,** 737–761.

Simmons, A. J., J. M. Wallace, and G. W. Branstator, 1983: Barotropic wave propagation and instability, and atmospheric teleconnections. *J. Atmos. Sci.,* **40,** 1363–1392.

Smith, T. M., R. W. Reynolds, R. E. Livezey, and D. C. Stokes, 1996: Reconstruction of historical sea surface temperature using empirical orthogonal functions. *J. Climate,* **9,** 1403–1420.

Tibaldi, S., and F. Molteni, 1990: On the operational predictability of blocking. *Tellus, Ser. A,* **42,** 343–365.

Tracton, M. S., K. Mo, W. Chen, E. Kalnay, R. Kistler, and G. White, 1989: Dynamical extended range forecasting (DERF) at the National Meteorological Center. *Mon. Wea. Rev.,* **117,** 1604–1635.

Trenberth, K. E., 1985: Potential predictability of geopotential heights over the Southern Hemisphere. *Mon. Wea. Rev.,* **113,** 54–64.

——, 1986: An assessment of the impact of transient eddies on the zonal flow during a blocking episode using localized Eliassen–Palm flux diagnostics. *J. Atmos. Sci.,* **43,** 2070–2087.

Tribbia, J. J., 1984: Modons in spherical geometry. *Geophys. Astrophys. Fluid Dyn.,* **30,** 131–168.

Verkley, W. T. M., 1984: The construction of barotropic modons on a sphere. *J. Atmos. Sci.,* **41,** 2492–2504.

von Storch, H., 1987: A statistical comparison with observations of control and El Niño simulations using the NCAR CCM. *Beitr. Phys. Atmos.,* **60,** 464–477.

White, G. H., 1980: Skewness, kurtosis and extreme values of Northern Hemisphere geopotential height. *Mon. Wea. Rev.,* **108,** 1446–1455.